Carbon 99 (2016) 466–471

Contents lists available at ScienceDirect

Carbon

journal homepage: www.elsevier.com/locate/carbon

Structural evolution of graphene in air at the electrical breakdown limit

Jangyup Son [a], Minkyung Choi [b], Heechae Choi [c], Sang Jin Kim [d, f], Seungchul Kim [c], Kwang-Ryeol Lee [c], Sanpon Vantasin [e], Ichiro Tanabe [e], Jongin Cha [a], Yukihiro Ozaki [e], Byung Hee Hong [d], In-Sang Yang [b, **], Jongill Hong [a, *]

[a] Department of Materials Science and Engineering, Yonsei University, 50 Yonsei, Seodaemun, Seoul 120-749, South Korea
[b] Department of Physics, Ewha Womans University, Daehyeon-dong, Seodaemun-gu, Seoul 120-750, South Korea
[c] Computational Science Center, Korea Institute of Science and Technology, 5, Hwarang-ro 14-gil, Seongbuk-gu, Seoul 136-791, South Korea
[d] SNU Graphene Center & Department of Chemistry, Seoul National University, Daehak-dong, Gwanak-gu, Seoul 151-747, South Korea
[e] Department of Chemistry, Kwansei Gakuin University, 2-1 Gakuen, Sanda, Hyogo 669-1337, Japan
[f] Soft Innovative Materials Research Center, Korea Institute of Science and Technology, Chudong-ro, 92, Bongdong-eup, Wanju-gun, Jeollabukdo 565-905, South Korea

ARTICLE INFO

Article history:
Received 11 August 2015
Received in revised form
26 November 2015
Accepted 30 November 2015
Available online 18 December 2015

ABSTRACT

In application of graphene to real electronics, understanding the mechanism of the electrical breakdown of the graphene in harsh environments should precede many activities in tamed conditions. In this article, we report the unusual structural evolution of microbridge graphene *in air* near the electrical current-breakdown limit. *In-situ* micro-Raman study revealed that Joule heating near the electrical breakdown gave rise to a substantial structural evolution: a previously unknown broad amorphous-like and partially reversible phase at an on- and off-current of ~3.0 × 10^8 A/cm^2, which finally drove the phase to the electrical current-breakdown. Our calculations suggest that the phase originates from the broken symmetry caused by defect formations during Joule heating. In particular, these formations are bonds of carbon-oxygen and vacancies-oxygen. A collection of energetically favorable vacancies-oxygen pairs results in porous graphene, and its evolution can be the key to understanding how the breakdown starts and propagates in graphene under high current density in air.

1. Introduction

Graphene, a single layer of graphite, has many electrical features that are not readily found in other materials, which makes it promising for future electronic devices [1–4]. Though research on graphene-based nanoelectronic applications has been extensive [5–9], the behavior of graphene in harsh environments is still ill understood. In particular, no significant progress has been made under harsh conditions such as under electrical current as high as that at which graphene starts to break down and under ambient conditions. Applications tested so far have not allowed observations at such extremes not only because of their poor design but also because of contamination introduced during fabrication. The breakdown of the graphene/metal contact due to the high contact resistance and stress concentration, for instance, has limited the study of the electrical behavior of graphene to currents far lower than those at which graphene itself reacts to the applied current [10–12]. In addition, most experiments on electrical measurements and surface control has been carried out at low temperature in vacuum, an ideal condition, rather than at room temperature in air. The gas species in air have kept researchers from examining graphene's electrical behavior at its breakdown limit.

Here, we report our observation of the unusual structural evolution of graphene *in air* as we increase current density to ~3.0 × 10^8 A/cm^2, which is near graphene's electrical breakdown limit. To the best of our knowledge, such high current density has never been applied at room temperature under ambient conditions. Our study was made possible by our unique design of microbridge graphene, and our observation of the structural evolution in conjunction with calculation results provides a vital clue to

* Corresponding author.
** Corresponding author.
E-mail addresses: yang@ewha.ac.kr (I.-S. Yang), hong.jongill@yonsei.ac.kr (J. Hong).

http://dx.doi.org/10.1016/j.carbon.2015.11.075
0008-6223/

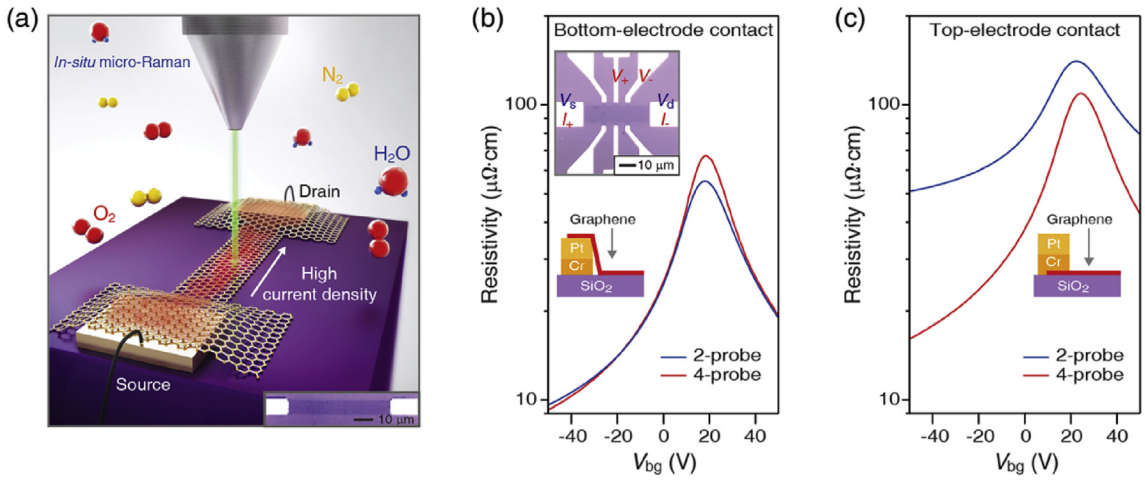

Fig. 1. (a) An illustration of the microbridge of single-layer graphene and *in-situ* micro-Raman measurements under an ambient condition. Change in resistivity as a function of back gate voltage (V_{bg}) in Hall patterns having (b) the bottom-electrode and (c) the top-electrode contact type. (A color version of this figure can be viewed online).

understanding the breakdown mechanism of graphene and carbon-based devices at room temperature under ambient conditions.

2. Experimental

2.1. Sample preparation

Single-layer graphene (SLG) sheets were prepared by chemical vapor deposition (CVD) on Cu foils, and each sheet was transferred onto a heavily p-doped Si substrate with 300 nm-thick SiO_2 on top [13,14]. Microbridge graphene (10 μm × 70 μm) and Hall devices were patterned by electron-beam lithography and O_2 plasma etching.

2.2. Raman spectroscopy and AFM analysis

In-situ micro-Raman measurements were performed on the microbridge graphene in air with electrical current in repeating on and off cycles [15]. Each acquisition time of the Raman measurements was 2 min with an off-current interval of about 2 min between each acquisition. *Ex-situ* micro-Raman scattering spectra were also acquired with the 514.5 nm line of an Ar ion laser as an excitation source (×90 magnification, 0.71 NA) [16]. The spatial resolution of micro-Raman spectroscopy was about 500 nm in diameter. Surface topology was acquired by noncontact mode atomic force microscopy (AFM) with a 45° angle between tip and sample surface using a silicon cantilever controlled by a 100 kHz tuning fork [16].

2.3. Computational simulation

We performed semi-classical molecular dynamics (MD) simulations using the Large-scale Atomic/Molecular Massively Parallel Simulator (LAMMPS) [17], to investigate the structural evolution during oxidation of graphene at 600 K. The simulation temperature was chosen to mimic the Joule heating caused by the application of current densities [5,6,15,18,19]. A reactive force field between oxygen and carbon was applied to determine the chemical reaction between them [20].

3. Results and discussion

3.1. Fabrication of the microbridge graphene and graphene/electrode contact

We were able to fabricate the microbridge graphene out of the large-scale chemical vapor deposited (CVD) graphene [13,14] by simple, one-step electron-beam lithography without additional deposition of a metal electrode as illustrated in Fig. 1a and Fig. S1 (Supplementary Information). This fabrication design allowed us to significantly reduce structural defects of graphene that are introduced by additional fabrication processes and to avoid thermal-stress concentration resulting from a rapid thermal cycle. In this study, we utilize our finding that graphene *on* Cr/Pt (a bottom-electrode contact type, C_B) has a contact resistance significantly smaller than that of graphene *under* Cr/Pt (a top-electrode contact type, C_T), as shown in Fig. 1b and c. In the case of C_B, the resistivity measured with a 2-probe method was close to that measured with a 4-probe method (Fig. 1b), i.e., contact resistance was significantly low in device with C_B. We supposed that low contact resistance in our device was resulted from large difference of workfunction between graphene and Pt electrode, which makes C_B suitable for studying electrical breakdown phenomena because its configuration can reduce the concentration of both Joule heating and thermal stress at the contact under the high current. As a result, our microbridge graphene was able to endure a current density of up to 3.0×10^8 A/cm^2 *in air* before the electrical breakdown occurred.

3.2. In-situ micro-Raman spectroscopy

We carried out *in-situ* micro-Raman spectroscopy on microbridge graphene in air as we applied electrical current in repeating on and off cycles until the graphene reached electrical breakdown. Raman spectra shown in Fig. 2a indicate the dramatic structural deformation of microbridge graphene induced by high current density. Note that the on-current Raman spectra of microbridge graphene experiencing high current density (ranging from 1.3 to 2.6×10^8 A/cm^2) were significantly different from the spectra at off-current. The peaks near the original D and G peaks of pristine graphene became broad and their intensities rapidly grew when the current density exceeded 2.0×10^8 A/cm^2. Graphene oxide also

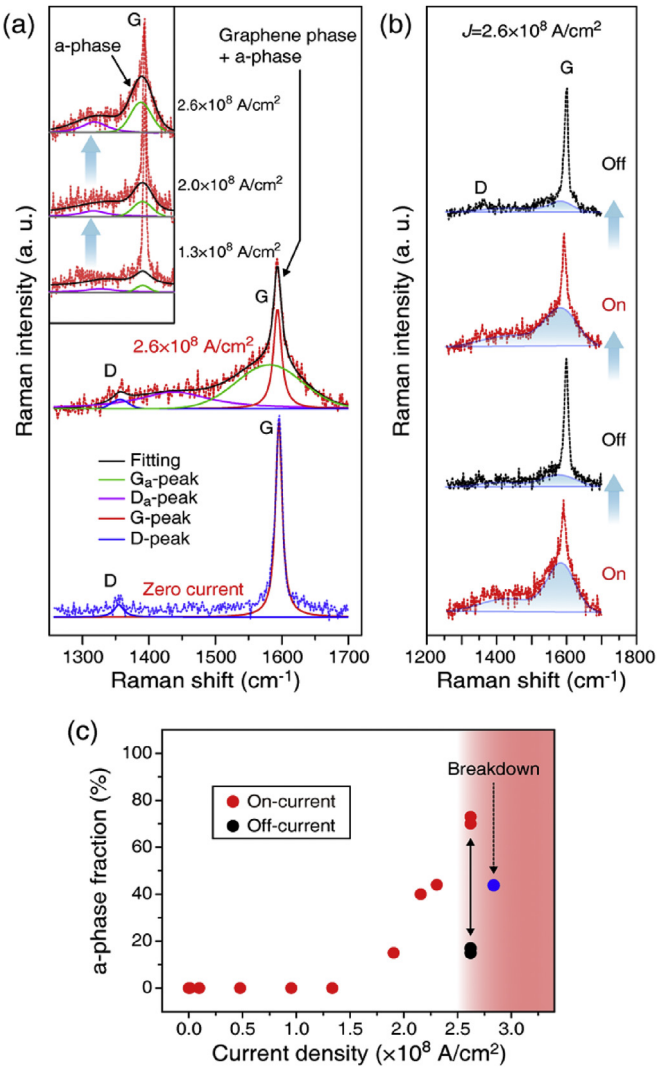

Fig. 2. (a) *In-situ* micro-Raman spectra measured under various current densities from 1.3×10^8 A/cm^2 to 2.6×10^8 A/cm^2. The blue curve is the Raman spectrum at the initial state (zero current), the red curve is the spectrum under the electrical current as indicated, and the black curves show the best fit of the Raman spectra. (b) Raman spectra under the high current density (2.6×10^8 A/cm^2), and the reversible change according to the electrical current being turned on and off. (c) The fraction of graphene and amorphous phase (labeled as a-phase in the figure), defined by the integrated intensity of the broad peaks divided by total integrated Raman intensity, under various current densities. Note that the amorphous phase fraction is partially reversible when the current is repeatedly turned on and off at 2.6×10^8 A/cm^2. After breakdown at 2.8×10^8 A/cm^2, the amorphous phase fraction was ~40%. (A color version of this figure can be viewed online)

shows such broad peaks, but the peak positions are at much higher wave numbers [21], which proves that the broad peaks observed in Fig. 2a are not caused by the formation of graphene oxide. They rather resemble the broad peaks found in amorphous carbon or fully disordered single layer graphene (SLG) [22–24]. For the purpose of discussion, we labeled the amorphous-like broad peaks near the D and G peaks of SLG D_a and G_a, respectively.

To our great surprise, we found those broad D_a and G_a peaks to be partially reversible, as shown in Fig. 2b. The intensity of the peaks became strong and dominant when a current density of 2.6×10^8 A/cm^2 was applied; when the current was off, the peaks were significantly diminished and some of them returned to the levels they had had just before the current was applied. This indicates that the changes in the D_a and G_a peaks were mostly due to the thermodynamically reversible deformation, including the possible oxygen migration [25]. The irreversible parts became larger as the intermittently applied on- and off-current remained at the high current density of 2.6×10^8 A/cm^2. In addition to the D_a and G_a peaks, the original narrow G peak was still observed at the G_a peak, implying that the microbridge graphene has two phases simultaneously, namely, the pristine graphene and the amorphous-like phase. The fraction of the amorphous-like phase, defined by the integrated intensity of the broad peaks divided by total integrated Raman intensity, rapidly increased when the applied current density exceeded 2.6×10^8 A/cm^2, as plotted in Fig. 2c. At this high current density, the symmetry of graphene can be broken because of the absorption of gas species in air and the resulting energy dissipations through phonon modes, which likely results in the broad D_a and G_a Raman peaks. Our previous study suggests that the broad peaks originate from the adsorbed oxygen on graphene and the resulting defects due to electro-thermal (or Joule) heating induced by high current density [15]. Oxygen is the second-most abundant molecule in air, and it is more reactive with carbon than nitrogen at temperatures below 700 K. Since the defect or distortion of graphene brought on by oxygen adatoms is localized, we were able to observe both pristine graphene and amorphous-like phases at the same time (more of this later). After electrical breakdown, the peaks of pristine graphene became prominent and the D_a and G_a peaks were significantly decreased.

3.3. Surface morphology of microbridge graphene by micro-Raman spectroscopy

Next, we focus our study on the surface morphology of microbridge graphene by micro-Raman spectroscopy before and after electrical breakdown. We used two samples of microbridge graphene. To the first sample (microbridge A in Fig. 3a), we applied a current density of 2.5×10^8 A/cm^2. The graphene did not break down, and a weak amorphous-like feature appeared. At the area near the graphene/metal contact the amorphous-like feature was somewhat more pronounced than it was at the area near the center of the microbridge. When we increased the current beyond 3.0×10^8 A/cm^2, the breakdown limit, in the second microbridge graphene (microbridge B in Fig. 3b), strong defect features were dominant and the D and D′ peaks were clearly confirmed. The D peak intensity in the vicinity of the contact was higher than the intensity at the center. Interestingly, the amorphous-like feature was substantially diminished in microbridge graphene B. The contrast in the I_D/I_G ratio mapping image of microbridge graphene acquired by micro-Raman spectroscopy was strong enough to reveal the difference in the ratio of $I_D/I_{D'}$ (not shown), the fingerprint of defect types in graphene, along the microbridge channel. The ratio of $I_D/I_{D'}$ was less than 7 in microbridge graphene B, which means that the defects are most likely vacancies [26]. It is therefore not unreasonable to deduce that vacancies or sizable voids were introduced in microbridge graphene B after the electrical breakdown. In fact, as we demonstrated by molecular dynamic simulation (discussed below), the area or site at which oxygen was absorbed can act as a nucleation site for the formation of vacancies and voids. We expect the amorphous-like phase to become significantly lessened due to the formation of vacancies or voids, which leads to wrinkles being flattened by stress relaxation. We believe that this is how the breakdown starts and propagates in microbridge graphene in air under the extreme current we applied.

3.4. Computational simulation for the electrical breakdown

We carried out molecular dynamics (MD) simulations to establish evidence of the mechanism for the electrical breakdown.

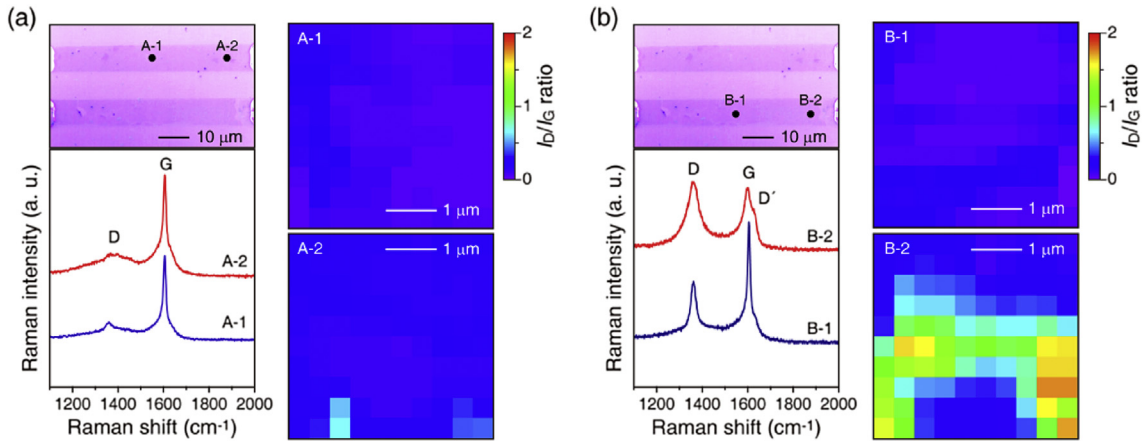

Fig. 3. (a) Raman spectra and micro-Raman I_D/I_G ratio mapping of the microbridge graphene heated at a current density of 2.5×10^8 A/cm^2 (microbridge graphene A), and those of the (b) microbridge graphene after electrical breakdown beyond 3.0×10^8 A/cm^2 (microbridge graphene B). (A color version of this figure can be viewed online)

Fig. 4a shows a typical snapshot of the simulation of oxidation of graphene for 6 ps at 600 K. The oxidation induced considerable distortions as well as defects, resulting in breaking the hexagonal network structure of graphene (see Video S1. (Supplementary Information)). The defects were vacancy-oxygen (V–O) and carbon-oxygen (C–O and C=O). As shown in the side view in Fig. 4a, the graphene has a strong tendency of being convex toward the surface oxygen, with the exception of the case of V–O. Based on the simulation, we investigated the energetics of three typical configurations, C–O, V–O, and C=O, by density functional theory (DFT) calculation as implemented in the Vienna Ab-initio Simulation Package (VASP) code (shown in Fig. 4b). Relatively high, positive values of the formation energy were obtained for various C–O cases. The C=O configuration, where the oxygen atoms were adsorbed at both sides of the graphene with a broken C–C bond, has a smaller but still positive value of the formation energy, which

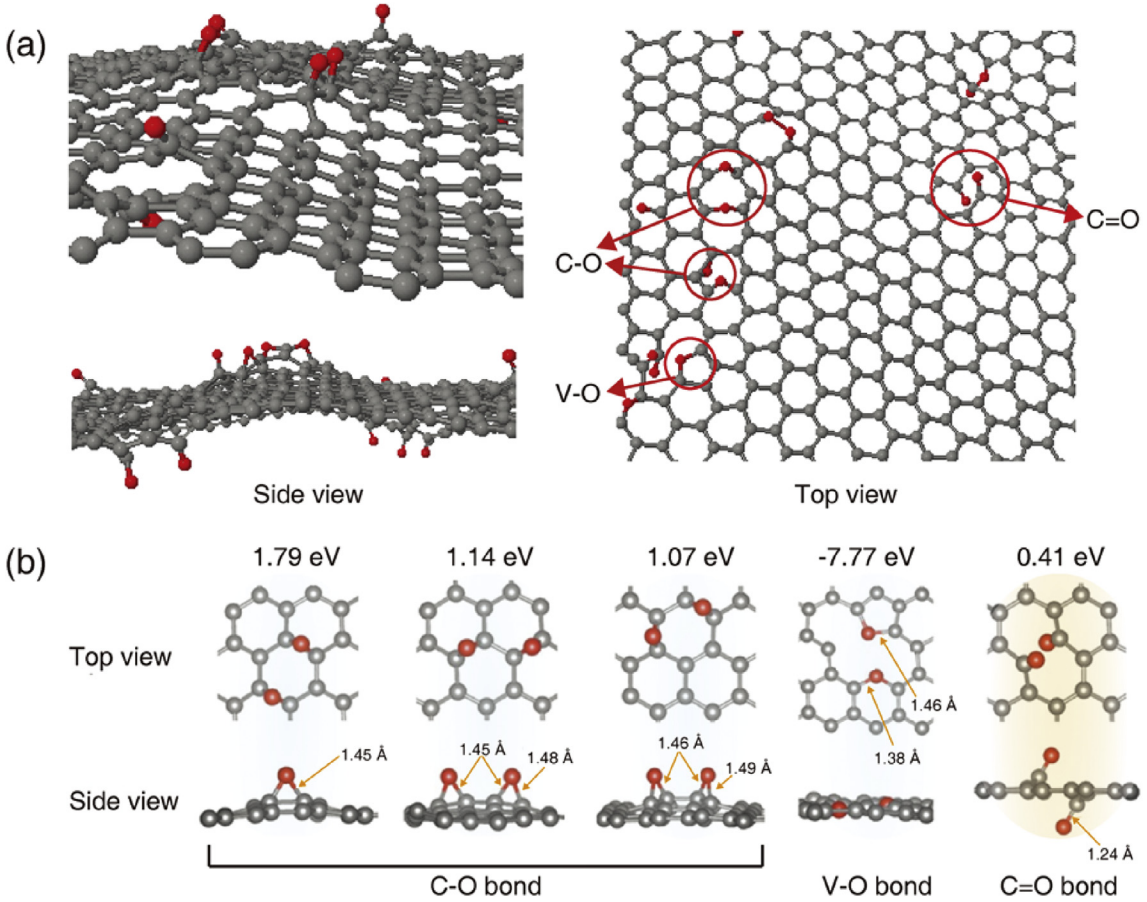

Fig. 4. (a) The snapshot of molecular dynamics (MD) simulation. Red spheres are oxygen atoms, and various oxidation configurations appear in the snapshot. (b) Top and side views of various oxygen bonding configurations and corresponding formation energies obtained by the DFT calculation; the energies are defined by the difference in energy between the configuration and the sum of the energies of unreacted graphene and oxygen molecules. (A color version of this figure can be viewed online)

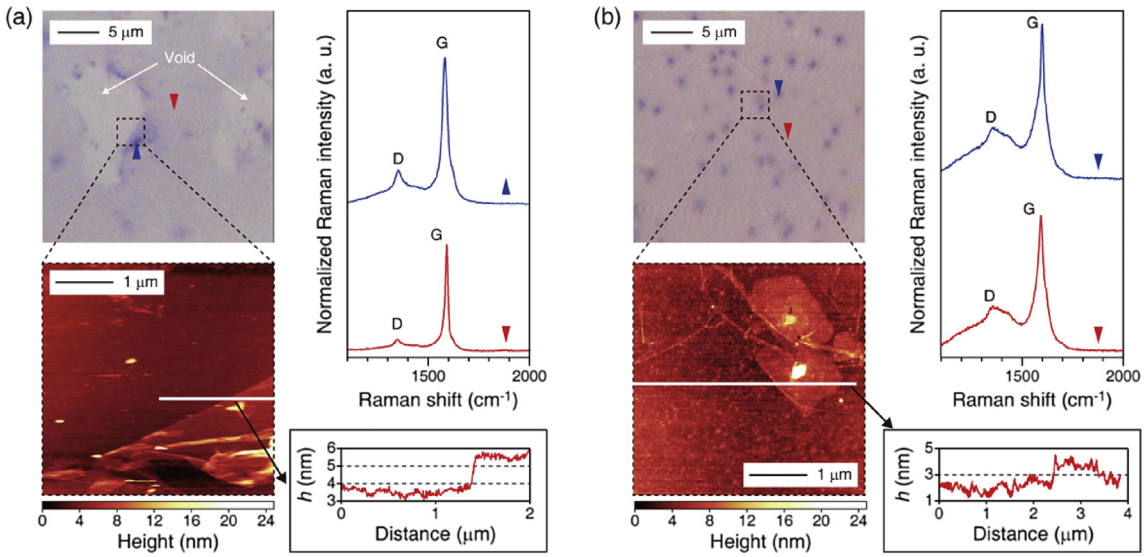

Fig. 5. (a) Graphene sheet heated in air. (b) Graphene sheet heated in Ar. The blue triangles mark the Raman spectra near the void; the red triangles mark the Raman spectra far away from the void (A color version of this figure can be viewed online)

is 0.41 eV. However, if the configurational entropy is considered, we found that this C═O bond can be thermodynamically stable. In fact, X-ray photoelectron microscopy (XPS) confirmed the existence of both C═O and C–O bonds, and the dominant population of the C–O bond in the microbridge graphene experiencing Joule heating [15]. Our calculations showed that the V–O configuration is energetically the most stable one among various C–O bonding configurations, with formation energy of −7.77 eV, and the V–O bond is so stable that the defects cannot be spontaneously eliminated. Hence, the irreversible part of broad Raman peaks we observed can be understood in terms of the leftover of the V–O bond in graphene, and surface characteristics in the microbridge graphene near the electrical breakdown limit in air can be attributed mainly to V–O configurations. In particular, this V–O configuration is considered to play a crucial role in the breakdown process.

Supplementary video related to this article can be found at http://dx.doi.org/10.1016/j.carbon.2015.11.075.

3.5. AFM analysis on graphene sheet heated in air and Ar

To provide evidence for our explanation of the electrical breakdown, we separately prepared two CVD graphene sheets and thermally heated them up to 773 K in air and in Ar, respectively, and again observed their surface characteristics by atomic force microscopy (AFM) and micro-Raman spectroscopy. Since non-uniform Joule heating at the contact is still difficult to avoid in microbridge graphene (see Fig. 3), we used large-area CVD graphene sheets in this experiment. Here, we focus on the experimental results obtained at 773 K because they provide a marked contrast between the two graphene sheets, which exemplifies the breakdown mechanism. We found that graphene heated in air showed sizeable voids and that some of it was rolled up near the edges of the voids, forming double-layered graphene, as shown in Fig. 5a. Indeed, micro-Raman spectra confirmed that the spots near the voids (see Raman spectrum marked with the blue triangular symbol in Fig. 5a) show an amorphous-like and a double-layered spectrum (see Fig. S2 (Supplementary Information)), which is consistent with our observations in microbridge graphene. In contrast, the Raman spectrum away from the voids (marked with the red triangular symbol in Fig. 5a) showed that the spectrum of the as-prepared pristine graphene had neither the amorphous-like structure nor the structural curvature. On the other hand, graphene heated in an Ar atmosphere did not show detectable voids by AFM (Fig. 5b). Instead, we found many spots on its surface, which as AFM and Raman spectroscopy confirmed, were composed of two or three layers of graphene. The number of a spot of graphene increased after heating in Ar, as shown in Fig. S3 (Supplementary Information). We think that these spots are formed when the carbon-based polymer residue on the graphene surface (left over after the CVD process) thermally decomposed during heating. In the case of graphene heated in air, these spots were absent because the residual polymer on graphene is easily removed by oxygen—the so-called ashing process. (This, too, is evidence that oxygen is active with graphene during heating.) Surface characterization by AFM also revealed that the surface away from the voids was flatter for graphene heated in air than it was for graphene heated in Ar. The flattening occurs because when the C–O bonds pop up in air to form voids or vacancies, the accumulated thermal stress is released and, as a result, wrinkles or structural curvatures are lessened. This explains the substantial diminishing of the amorphous-like feature in microbridge graphene B in Fig. 3b. Graphene externally heated in Ar does not have this mechanism of void creation releasing thermal stress and hence suffers from symmetry breaking due to crumpling of the surface. Graphene microbridges heated by electrical current in Ar also showed D_a and G_a peaks in Raman, see Fig. S4 (Supplementary Information), which is consistent with the fact that the Raman spectrum distant from the spots still contains the broad features near D and G peaks and that the height profile measured by AFM shows high surface curvatures, i.e., a rough surface (Fig. 5b). We concluded based on such evidence that the reversible part in the broad Raman peaks was originated from physical changes due to the thermal stress, and the irreversible part was from chemical changes in the amorphous-like carbon phase.

4. Conclusions

In conclusion, our microbridge graphene reached electrical breakdown in air, which results in an open circuit, immediately after we applied a current density of ~3.0×10^8 A/cm^2. Our experimental and simulation results lead us to conclude that oxygen reacting with pristine graphene is responsible for the electrical breakdown of graphene and that the most likely structure

satisfying this electrical breakdown is porous graphene with V–O bonds. When the porous structures become dominant and connected to one another to form voids, they can initiate the path for, or trigger, the breakdown of the graphene. We believe that this is how the breakdown starts and propagates in graphene under high current density in air. Our finding should benefit the application of graphene in real electronics.

Acknowledgments

Research at Yonsei University was supported in part by Samsung Electronics Co., by Basic Science Research Program (2014R1A2A1A11050290 and 2013R1A1A2013745) through the National Research Foundation of Korea (NRF) funded by the Korean government (MOE and MSIP), by the National Research Foundation of Korea (NRF) grant funded by the Korea government (MSIP) (NRF-2014R1A2A1A11050290), and by Creative Materials Discovery Program through the National Research Foundation of Korea (NRF) funded by the Ministry of Science, ICT and Future Planning (2015M3D1A1070465). Research at Ewha University was supported in part by the NRF Grant (No. 2015001948) and the Joint Research Project under the Korea-Japan Basic Scientific Cooperation Program (2013K2A2A4003603). Work at KIST was supported by the Industrial Strategic Technology Development Program (Grant No. 10041589) funded by the MOTIE of Korea and KIST Institutional Project (2E25372). Work at Seoul National University was supported in part by the Global Research Lab (GRL) Program (2011-0021972) through the NRF funded by the Korean government (MEST and MKE).

Appendix A. Supplementary data

Supplementary data related to this article can be found at http://dx.doi.org/10.1016/j.carbon.2015.11.075.

References

[1] K.S. Novoselov, A.K. Geim, S.V. Morozov, D. Jiang, Y. Zhang, S.V. Dubonos, et al., Electrical field effect in atomically thin carbon films, Science 306 (2004) 666–669.
[2] K.S. Novoselov, A.K. Geim, S.V. Morozov, D. Jiang, M.I. Katsnelson, I.V. Grigorieva, S.V. Dubonos, et al., Two-dimensional gas of massless Dirac fermions in graphene, Nature 438 (2005) 197–200.
[3] Y. Zhang, Y.W. Tan, H.L. Stormer, P. Kim, Experimental observation of the quantum Hall effect and Berry's phase in graphene, Nature 438 (2005) 201–204.
[4] A.H.C. Neto, F. Guinea, N.M.R. Peres, K.S. Novoselov, A.K. Geim, The electronic properties of graphene, Rev. Mod. Phys. 81 (2009) 109–162.
[5] X. Wang, X. Li, L. Zhang, Y. Yoon, P.K. Weber, H. Wang, et al., N-doping of graphene through electrothermal reactions with ammonia, Science 324 (2009) 768–771.
[6] X. Jia, M. Hofmann, V. Meunier, B.G. Sumpter, J. Campos-Delgado, J.M. Romeo-Herrera, et al., Controlled formation of sharp zigzag and amchair edges in graphitic nanoribbons, Science 323 (2009) 1701–1705.
[7] R. Murali, Y. Yang, K. Brenner, T. Beck, J.D. Meindl, Breakdown current density of graphene nanoribbons, Appl. Phys. Lett. 94 (2009) 243114.
[8] P. Avouris, Graphene: electronic and photonic properties and devices, Nano Lett. 10 (2010) 4285–4294.
[9] P. Joshi, H.E. Romero, A.T. Neal, V.K. Toutam, S.A. Tadigadapa, Intrinsic doping and gate hysteresis in graphene field effect devices fabricated on SiO_2 substrates, J. Phys. Condens Matter 22 (2010) 334214.
[10] E.J.H. Lee, K. Balasubramanian, R.T. Weitz, B. Marko, K. Kern, Contact and edge effects in graphene devices, Nat. Nanotechnol. 3 (2008) 486–490.
[11] K. Nagashio, T. Nishimura, K. Kita, A. Toriumi, Contact resistivity and current flow path at metal/graphene contact, Appl. Phys. Lett. 97 (2010) 143514.
[12] D. Yoon, Y.W. Son, H. Cheong, Negative thermal expansion coefficient of graphene measured by Raman spectroscopy, Nano Lett. 11 (2011) 3227–3231.
[13] K.S. Kim, Y. Zhao, H. Jang, S.Y. Lee, J.M. Kim, K.S. Kim, et al., Large-scale pattern growth of graphene films for stretchable transparent electrodes, Nature 457 (2009) 706–710.
[14] S. Bae, H. Kim, Y. Lee, X. Xu, J.S. Park, Y. Zheng, et al., Roll-to-roll production of 30-inch graphene films for transparent electrodes, Nat. Nanotechnol. 5 (2010) 574–578.
[15] M. Choi, J. Son, H. Choi, H.J. Shin, S. Lee, S. Kim, et al., In-situ Raman spectroscopy of current-carrying graphene microbridge, J. Raman Spectrosc. 45 (2014) 168–172.
[16] S. Vantasin, I. Tanabe, Y. Tanaka, T. Itoh, T. Suzuki, Y. Kutsuma, et al., Tip-enhanced Raman scattering of the local nanostructure epitaxial graphene grown on 4H-SiC (0001), J. Phys. Chem. C 118 (2014) 25809–25815.
[17] S. Plimpton, Fast parallel algorithms for short-range molecular dynamics, J. Comp. Phys. 117 (1995) 1–19.
[18] J. Moser, A. Barreiro, A. Bachtold, Current-induced cleaning of graphene, Appl. Phys. Lett. 91 (2007) 163513.
[19] I. Calizo, A.A. Balandin, W. Bao, F. Miao, C.N. Lau, Temperature dependence of the Raman spectra of graphene and graphene multilayers, Nano Lett. 7 (2007) 2645–2649.
[20] J.C. Fogarty, H.M. Aktulga, A.Y. Grama, A.C. van Duin, S.A. Pandit, A reactive molecular dynamics simulation of the silica-water interface, J. Chem. Phys. 132 (2010) 174704.
[21] K.N. Kudin, B. Ozbas, H.C. Schniepp, R.K. Prud'homme, I.A. Aksay, R. Car, Raman spectra of graphite oxide and functionalized graphene sheets, Nano Lett. 8 (2008) 36–41.
[22] M.A. Tamor, W.C. Vassell, Raman fingerprinting of amorphous carbon films, J. Appl. Phys. 76 (1994) 3823.
[23] J. Schwan, S. Ulrich, V. Batori, H. Ehrhardt, Raman spectroscopy on amorphous carbon films, J. Appl. Phys. 80 (1996) 440.
[24] A.C. Ferrari, J. Robertson, Interpretation of Raman spectra of disordered and amorphous carbon, Phys. Rev. B 61 (2000) 14095.
[25] S.K. Hong, J.E. Kim, S.O. Kim, B.J. Cho, Analysis on switching mechanism of graphene oxide resistive memory device, J. Appl. Phys. 110 (2011) 044506.
[26] A. Eckmann, A. Felten, A. Mishchenko, L. Britnell, R. Krupke, K.S. Novoselov, et al., Probing the nature of defects in graphene by Raman spectroscopy, Nano Lett. 12 (2012) 3925–3930.